Flattening of a Curved-Surface Buckybowl (Corannulene) by η^6 Coordination to $\{Cp^*Ru\}^+$

Paul A. Vecchi,† Celedonio M. Alvarez,† Arkady Ellern,† Robert J. Angelici,*,† Andrzej Sygula,‡ Renata Sygula,‡ and Peter W. Rabideau‡

Ames Laboratory and Department of Chemistry, Iowa State University, Ames, Iowa 50011-3111, and Department of Chemistry, Mississippi State University, Mississippi State, Mississippi 39762

Received June 29, 2005

The corannulene complex $[Cp^*Ru(\eta^6\text{-}C_{20}H_{10})]^+$ (**3**$^+$; where $Cp^* = \eta^5\text{-}C_5Me_5$), prepared by the reaction of $[Cp^*Ru(\mu_3\text{-}Cl)]_4$ with Ag^+ and the curved-surface buckybowl $C_{20}H_{10}$ (**1**), has a structure in which the bowl is slightly flattened as compared with the case for free corannulene. The corannulene unit in $[(Cp^*Ru)_2(\mu_2\text{-}\eta^6\text{:}\eta^6\text{-}C_{20}H_{10})][PF_6]_2$ (**4**$[PF_6]_2$), containing two $\eta^6\text{-}\{Cp^*Ru\}^+$ units coordinated on opposite sides of the corannulene, is flattened substantially more. The X-ray-determined structure of the corresponding SbF_6^- salt, $[(Cp^*Ru)_2(\mu_2\text{-}\eta^6\text{:}\eta^6\text{-}C_{20}H_{10})][SbF_6]_2$ (**4**$[SbF_6]_2$), shows that the corannulene bowl is almost completely flat. Low-temperature NMR studies of the analogous 1,2,5,6-tetramethylcorannulene complex $[(Cp^*Ru)_2(\mu_2\text{-}\eta^6\text{:}\eta^6\text{-}C_{20}H_6Me_4)]^{2+}$ (**6**$^{2+}$) show that there is a very low barrier to inversion of the bowl, even at −90 °C. Computational investigations reproduce the major structural features of **3**$^+$ and **4**$^{2+}$ and account for the low corannulene inversion barrier in **4**$^{2+}$.

Introduction

The discovery of buckminsterfullerene (C_{60}),[1] commonly known as "buckyball", in the 1980s has led to a renewed interest in the chemistry of curved carbon surfaces. Those compounds that have carbon frameworks that can be identified on the surface of C_{60} have been termed "buckybowls".[2] Buckybowl compounds differ from traditional polyaromatic hydrocarbons in that they are strained (curved) and have both concave and convex surfaces. The smallest buckybowl is corannulene ($C_{20}H_{10}$, **1**), which may be described as the cap of C_{60}. It

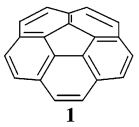

1

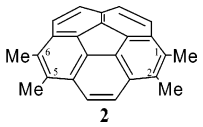

2

was first prepared in 1966 by a multistep reaction sequence.[3] Its molecular structure was determined in 1976,[4] confirming the curved nature of corannulene. The difficulty and overall low yields of the synthesis discouraged further investigations of **1**. Recently, improved syntheses[5] have enabled more extensive studies of its chemistry and reactivity.

Although both C_{60} and corannulene are curved carbon surfaces, they exhibit very different reactivities. In transition-metal complexes of C_{60},[6] the metal is always bonded in an η^2 fashion to two carbon atoms, and although C_{60} contains 20 six-membered rings, there are no reported examples of a complex in which C_{60} is η^6 coordinated to a transition metal. In the first reported transition-metal complexes of corannulene (**1**) and 1,2,5,6-tetramethylcorannulene (**2**), the metal fragments are η^6 bound to the carbon atoms of a six-membered

* To whom correspondence should be addressed. Tel: 515-294-2603. Fax: 515-294-0105. E-mail: angelici@iastate.edu.
† Iowa State University.
‡ Mississippi State University.

(1) (a) Kroto, H. W.; Heath, J. R.; O'Brien, S. C.; Curl, R. F.; Smalley, R. E. *Nature* **1985**, *318*, 162. (b) Heath, J. R.; O'Brien, S. C.; Curl, R. F.; Kroto, H. W.; Smalley, R. E. *Comments Condens. Mater. Phys.* **1987**, *13*, 119. (c) Kroto, H. W.; *Nature* **1987**, *329*, 529. (d) Kraetschmer, W.; Lamb, L. D.; Fostiropoulos, K.; Huffman, D. R. *Nature* **1990**, *347*, 354.

(2) (a) Rabideau, P. W.; Abdourazak, A. H.; Folsom, H. E.; Marcinow, Z.; Sygula, A.; Sygula, R. *J. Am. Chem. Soc.* **1995**, *117*, 6410. (b) Abdourazak, A. H.; Marcinow, Z.; Sygula, A.; Sygula, R.; Rabideau, P. W. *J. Am. Chem. Soc.* **1995**, *117*, 6410. (c) Rabideau, P. W.; Sygula, A. *Acc. Chem. Res.* **1996**, *29*, 235.

(3) (a) Barth, W. E.; Lawton, R. G. *J. Am. Chem. Soc.* **1966**, *88*, 380. (b) Lawton, R. G.; Barth, W. E. *J. Am. Chem. Soc.* **1971**, *93*, 1730.

(4) (a) Hanson, J. C.; Nordman, C. E. *Acta Crystallogr., Sect. B* **1976**, *B32*, 1147. (b) Petrukhina, M. A.; Andreini, K. W.; Mack, J.; Scott, L. T. *J. Org. Chem.* **2005**, *70*, 5713.

(5) (a) Sygula, A.; Xu, G.; Marcinow, Z.; Rabideau, P. W. *Tetrahedron* **2001**, *57*, 3637 and references therein. (b) Scott, L. T.; Cheng, P.-C.; Hashemi, M. M.; Bratcher, M. S.; Meyer, D. T.; Warren, H. B. *J. Am. Chem. Soc.* **1997**, *119*, 10963 and references therein. (c) Seiders, T. J.; Baldridge, K. K.; Elliott, E. L.; Grube, G. H.; Siegel, J. S. *J. Am. Chem. Soc.* **1999**, *121*, 7439. (d) Seiders, T. J.; Elliott, E. L.; Grube, G. H.; Siegel, J. S. *J. Am. Chem. Soc.* **1999**, *121*, 7804 (e) Jones, C. S.; Elliot, E. L.; Siegel, J. S. *Synlett* **2004**, 187.

(6) For examples see: (a) Lee, K.; Choi, Y. J.; Cho, Y.-J.; Lee, C. Y.; Song, H.; Lee, C. H.; Lee, Y. S.; Park, J. T.; *J. Am. Chem. Soc.* **2004**, *126*, 9837. (b) Song, L.-C.; Yu, G.-A.; Su, F.-H.; Hu, Q.-M. *Organometallics* **2004**, *23*, 4192. (c) Song, L.-C.; Wang, G.-F.; Liu, P.-C.; Hu, Q.-M. *Organometallics* **2003**, *22*, 4593. (d) Lee, K.; Song, H.; Kim, B.; Park, J. T.; Park, S.; Choi, M.-G. *J. Am. Chem. Soc.* **2002**, *124*, 2872. (e) Song, L.-C.; Liu, J.-T.; Hu, Q.-M.; Weng, L.-H. *Organometallics* **2000**, *19*, 1643. (f) Balch, A. L.; Olmstead, M. M. *Chem. Rev.* **1998**, *98*, 2123. (g) Hsu, H.-F.; Shapley, J. R. *J. Am. Chem. Soc.* **1996**, *118*, 9192. (h) Fagan, P. J.; Calabrese, J. C.; Malone, B. *Science* **1991**, *252*, 1160. (i) Hirsch, A.; Bretbreich, M. *Fullerenes: Chemistry and Reactions*; Wiley-VCH: Weinheim, Germany, 2005.

10.1021/om0505458 CCC: $30.25
Publication on Web 08/09/2005

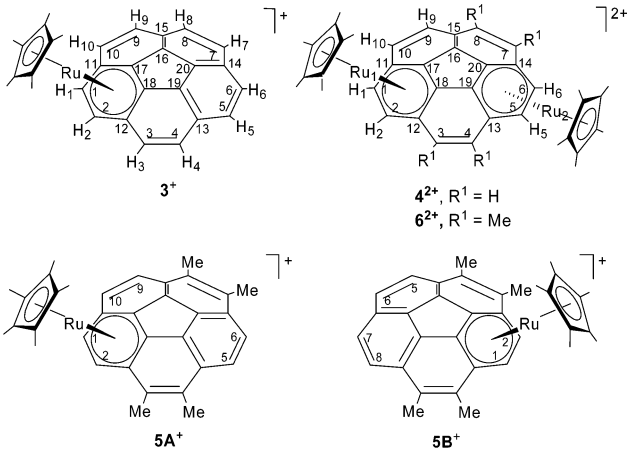

Figure 1. Atom-labeling schemes for the corannulene ligand in $\mathbf{3}^+$, $\mathbf{4}^{2+}$, $\mathbf{5A}^+$, $\mathbf{5B}^+$, and $\mathbf{6}^{2+}$.

ring.[7−9] More recently, the η^2 corannulene complexes $[[Rh_2(O_2CCF_3)_4]_m\cdot(C_{20}H_{10})_n]$ (m:n = 1:1, 3:2) were prepared by a gas-phase deposition method.[10] An X-ray structural investigation of these compounds showed that the Rh_2 units are η^2 coordinated to both the exo and endo sides of the corannulene in one- and two-dimensional arrays. The structures of the corannulene units in the compounds were not significantly different from that of free corannulene.[4] Dissolution of the compounds in acetone led to the dissociation of corannulene from the Rh_2 unit. Very recently, AgX complexes of corannulene were characterized by X-ray diffraction.[11] Depending on the X^- anion (ClO_4^-, $CF_3SO_3^-$, BF_4^-), the compounds exist as one- or two-dimensional networks in which Ag^+ and corannulene are linked by η^2 and η^1 coordination; the structure of the corannulene unit is changed very little from that of free corannulene.

We recently communicated the synthesis and X-ray structural characterization of $[(Cp^*Ru)_2(\mu_2\text{-}\eta^6\text{:}\eta^6\text{-}C_{20}H_{10})][PF_6]_2$ ($\mathbf{4}[PF_6]_2$; $Cp^* = \eta^5\text{-}C_5Me_5$).[9] The structural results showed that the two $\{Cp^*Ru\}^+$ fragments are η^6 bound to nonadjacent rings on opposite sides of the corannulene (Figure 1). Significant flattening of the corannulene ligand upon coordination of the $\{Cp^*Ru\}^+$ units was observed, and structural parameters indicated that the exo $\{Cp^*Ru\}^+$ unit was bound differently than the endo $\{Cp^*Ru\}^+$ moiety to the corannulene. Solution NMR studies of $\mathbf{4}[PF_6]_2$ showed that the corannulene unit undergoes rapid inversion at room temperature. In this report, we describe the dramatic effect of one and two η^6-$\{Cp^*Ru\}^+$ groups on the shape of the corannulene ligand in $[Cp^*Ru(\eta^6\text{-}C_{20}H_{10})][SbF_6]$ ($\mathbf{3}[SbF_6]$) and $[(Cp^*Ru)_2(\mu_2\text{-}\eta^6\text{:}\eta^6\text{-}C_{20}H_{10})][SbF_6]_2$ ($\mathbf{4}[SbF_6]_2$) (Figure 1), the effect of $\{Cp^*Ru\}^+$ on lowering the barrier for corannulene inversion, and computational studies that provide a fundamental basis for understanding these structural and fluxional effects.

Experimental Section

General Considerations. All reactions were carried out under an atmosphere of dry argon using standard Schlenk techniques. Methylene chloride (CH_2Cl_2), diethyl ether (Et_2O), and hexanes were purified on alumina using a Solv-Tek solvent purification system. Methylene chloride-d_2 (CD_2Cl_2) was refluxed overnight with calcium hydride, distilled, and subjected to three freeze−pump−thaw cycles before use. Nitromethane-d_3 (CD_3NO_2) was purchased from Aldrich and subjected to three freeze−pump−thaw cycles before use. Corannulene,[5a] 1,2,5,6-tetramethylcorannulene,[5a] and $[Cp^*Ru(\mu_3\text{-}Cl)]_4$[12] were synthesized by following published methods. The complexes $[(Cp^*Ru)_2(\mu_2\text{-}\eta^6\text{:}\eta^6\text{-}C_{20}H_{10})][X]_2$, where $X = BF_4^-$, PF_6^-, were synthesized as reported previously.[9] All other chemicals ($AgBF_4$, $AgPF_6$, $AgSbF_6$; 99.99+%) were used without further purification as purchased from Aldrich. Filtrations were performed through a small plug of filter paper, Celite, and cotton, and the solutions were transferred via thin-wall, 18 gauge, Teflon tubing (Alpha Wire Corp.). All of the $\{Cp^*Ru\}^+$ complexes of **1** and **2** are sensitive to moisture and more difficult to handle during a humid summer. They are stable for hours when exposed to dry air both in the solid state and in CD_3NO_2 solution.

Solution NMR spectra were obtained on a Bruker DRX-400 spectrometer using either CD_3NO_2 or CD_2Cl_2 as the solvent, internal lock, and internal reference (δ 4.33 (^{1}H), 62.8 (^{13}C) and δ 5.32 (^{1}H), 54.0 (^{13}C), respectively). Electrospray ionization mass spectra were obtained on a Finnigan TSQ700 triple-quadrupole mass spectrometer (Finnigan MAT, San Jose, CA) fitted with a Finnigan ESI interface. Elemental analyses were performed on a Perkin-Elmer 2400 series II CHNS/O analyzer.

Synthesis of $[Cp^*Ru(\eta^6\text{-}C_{20}H_{10})][X]$ ($\mathbf{3}[BF_4]$, $\mathbf{3}[PF_6]$, $\mathbf{3}[SbF_6]$). To a flask containing freshly prepared $[Cp^*Ru(\mu_3\text{-}Cl)]_4$ (11.0 mg, 0.0101 mmol), corannulene (**1**; 10.2 mg, 0.0408 mmol), and $AgBF_4$, $AgPF_6$, or $AgSbF_6$ (0.0420 mmol) was added 1 mL of CD_3NO_2. The solution was stirred at room temperature for 15 min, and the AgCl precipitate was removed by filtration. The resulting orange solution was evaporated to dryness under vacuum to give an oily residue of **3**[X]. These reactions are nearly quantitative, as indicated by NMR spectroscopy. The dark orange residue was then washed with diethyl ether (2 × 3 mL) and dried under vacuum. After **3**[X] was dissolved in 1−2 mL of CH_2Cl_2, the resulting solution was then filtered into 5 mL of hexanes to give orange powders of $[Cp^*Ru(\eta^6\text{-}C_{20}H_{10})][X]$ (23.2 mg, 91% yield, for $\mathbf{3}[PF_6]$; yields of the BF_4^- and SbF_6^- salts were similarly high). Anal. Calcd for $\mathbf{3}[SbF_6]\cdot 2H_2O$: C, 47.51; H, 3.85. Found: C, 47.01; H, 3.71. The solution NMR spectrum of $\mathbf{3}[PF_6]$ is very similar to that of $[Cp^*Ru(\eta^6\text{-}C_{20}H_{10})][O_3SCF_3]$ prepared via a different route and identified by its NMR spectra.

Synthesis and Characterization of $[(Cp^*Ru)_2(\mu_2\text{-}\eta^6\text{:}\eta^6\text{-}C_{20}H_{10})][SbF_6]_2$ ($\mathbf{4}[SbF_6]_2$). To a flask containing freshly prepared $[Cp^*Ru(\mu_3\text{-}Cl)]_4$ (22.0 mg, 0.0202 mmol), corannulene (**1**; 10.0 mg, 0.0400 mmol), and $AgSbF_6$ (28.5 mg, 0.0830 mmol) was added 1 mL of CD_3NO_2. The solution was stirred at room temperature for 1 h, and the AgCl precipitate was removed by filtration. The resulting dark orange solution was evaporated to dryness under vacuum to give a residue of $\mathbf{4}[SbF_6]_2$. These reactions are nearly quantitative, as indicated by NMR spectroscopy. The dark orange residue was dissolved in 5 mL of CH_2Cl_2 and filtered into 10 mL of hexanes to give $\mathbf{4}[SbF_6]_2$ (39.1 mg, 82% yield) as an orange solid. The ^{1}H NMR spectrum of the compound was nearly identical with that reported previously for $[(Cp^*Ru)_2(\mu_2\text{-}\eta^6\text{:}\eta^6\text{-}C_{20}H_{10})][BF_4]_2$ ($\mathbf{4}[BF_4]_2$).[9]

Synthesis and Characterization of $[Cp^*Ru(\eta^6\text{-}C_{20}H_6Me_4)][X]$ ($\mathbf{5}[BF_4]$, $\mathbf{5}[PF_6]$, $\mathbf{5}[SbF_6]$). To a flask containing freshly prepared $[Cp^*Ru(\mu_3\text{-}Cl)]_4$ (11.0 mg, 0.0101 mmol),

(7) Seiders, T. J.; Baldridge, K. K.; O'Connor, J. M.; Siegel, J. S. *J. Am. Chem. Soc.* **1997**, *119*, 4781.
(8) Alvarez, C. M.; Angelici, R. J.; Sygula, A.; Sygula, R.; Rabideau, P. W. *Organometallics* **2003**, *22*, 624.
(9) Vecchi, P. A.; Alvarez, C. M.; Ellern, A.; Angelici, R. J.; Sygula, A.; Sygula, R.; Rabideau, P. W. *Angew. Chem., Int. Ed.* **2004**, *43*, 4497.
(10) Petrukhina, M. A.; Andreini, K. W.; Mack, J.; Scott, L. T. *Angew. Chem., Int. Ed.* **2003**, *42*, 3375.
(11) Elliott, E. L.; Hernández, G. A.; Linden, A.; Siegel, J. S. *Org. Biomol. Chem.* **2005**, *3*, 407.
(12) Fagan, P. J.; Ward, M. D.; Calabrese, J. C. *J. Am. Chem. Soc.* **1989**, *111*, 1698.

1,2,5,6-tetramethylcorannulene (**2**; 12.5 mg, 0.0408 mmol), and $AgBF_4$, $AgPF_6$, or $AgSbF_6$ (0.0420 mmol) was added 1 mL of CD_3NO_2. The solution was stirred at room temperature for 15 min, and the AgCl precipitate was removed by filtration. The resulting dark orange solution was evaporated to dryness under vacuum. The residue was washed with diethyl ether (2 × 3 mL) and dried under vacuum to give [Cp*Ru(η^6-$C_{20}H_6Me_4$)][X] (25.0 mg, 90% yield for **5**[PF_6]) as an orange solid consisting of two isomers, $\mathbf{5A}^+$ and $\mathbf{5B}^+$ (see Figure 1 for labeling scheme), in a 2:1 ratio. Sometimes the dark orange residue was oily; orange powders could often be obtained by dissolving the residue in 1−2 mL of CH_2Cl_2 and filtering into 5 mL of hexanes. Slow cooling of a CH_2Cl_2 solution (or slow diffusion of diethyl ether into a CH_2Cl_2 solution) at −25 °C with careful exclusion of H_2O also yielded solid products, although the $\mathbf{5A}^+$:$\mathbf{5B}^+$ isomer ratio in the solid product was different after each recrystallization. This enrichment of one isomer over the other aided in chemical shift assignments to the two isomers. ^{1}H NMR (400.13 MHz, CD_3NO_2, room temperature, **5A**[SbF_6]): δ 8.23 (d, ^3J(H,H) = 9.2 Hz, 1H, H9), 8.07 (d, ^3J(H,H) = 8.8 Hz, 1H, H6), 7.94 (d, ^3J(H,H) = 8.8 Hz, 1H, H5), 7.62 (d, ^3J(H,H) = 9.2 Hz, 1H, H10), 6.46−6.42 (AB quartet, ^3J(AB) = 5.8 Hz, 2H, H1 and H2), 2.83 (d, ^5J(H,H) = 0.8 Hz, 3H, Me), 2.75 (s, 3H, Me), 2.73 (s, 3H, Me), 2.62 (q, ^5J(H,H) = 0.8 Hz, 3H, Me), 1.25 (s, 15H, Cp*) ppm. ^{13}C{^{1}H} NMR (100.61 MHz, CD_3NO_2, room temperature, **5A**[SbF_6]): δ 84.47 and 98.55 (C1 and C2); 82.10, 94.90, 97.00, 101.59 (Ru−C); 125.55, 127.74, 128.66, 133.16 (C5, C6, C9, C10); 140.86, 137.97, 137.03, 136.49, 134.94, 134.74, 134.06, 133.70, 133.28, 130.64 (non-hydrogen-containing C not bonded to Ru, $C_{20}H_6Me_4$); 15.94, 15.90, 15.68, 15.41 ($C_{20}H_6\mathit{Me}_4$); 94.55, 9.60 (C_5Me_5). ^{1}H NMR (400.13 MHz, CD_3NO_2, room temperature, **5B**[SbF_6]): δ 8.05 (d, ^3J(H,H) = 8.8 Hz, 2H, H6,7), 7.98 (d, ^3J(H,H) = 8.8 Hz, 2H, H5,8), 6.45 (s, 2H, H1,2), 2.83 (d, ^5J(H,H) = 0.8 Hz, 6H, Me), 2.61 (d, ^5J(H,H) = 0.8 Hz, 6H, Me), 1.37 (s, 15H, Cp*) ppm. ^{13}C{^{1}H} NMR (100.61 MHz, CD_3NO_2, room temperature, **5B**[SbF_6]): δ 15.97, 15.78 ($C_{20}H_6\mathit{Me}_4$), 94.82, 9.95 (C_5Me_5). The carbons of the corannulene ligand in **5B**[SbF_6] could not be fully assigned because its weak peaks were obscured by those of **5A**[SbF_6]. For comparison, the ^{1}H and ^{13}C NMR spectra of **2** are given. ^{1}H NMR (400.13 MHz, CD_3NO_2, room temperature): δ 8.00 (s, 2H), 7.97 (d, ^3J(H,H) = 8.8 Hz, 2H), 7.86 (d, ^3J(H,H) = 8.8 Hz, 2H) 2.746, 2.742 (2 s, 12 H). ^{13}C{^{1}H} NMR (100.61 MHz, CD_3NO_2, room temperature): δ 136.32, 134.87, 134.50, 134.37, 134.05, 132.96, 132.14, 130.71, 128.11, 126.21, 125.99, 15.15, 15.12.

Synthesis and Characterization of [(Cp*Ru)$_2$(μ_2-η^6:η^6-$C_{20}H_6Me_4$)][X]$_2$ (6[BF_4]$_2$, 6[PF_6]$_2$, 6[SbF_6]$_2$). To a flask containing freshly prepared [Cp*Ru(μ_3-Cl)]$_4$ (25.0 mg, 0.0230 mmol), 1,2,5,6-tetramethylcorannulene (**2**; 13.5 mg, 0.0441 mmol), and $AgBF_4$, $AgPF_6$, or $AgSbF_6$ (0.0950 mmol) was added 1 mL of CD_3NO_2. The solution was stirred for 1 h at room temperature, and the AgCl precipitate was removed by filtration. The dark orange solution was evaporated to dryness under vacuum. The residue was washed with diethyl ether and dried under vacuum to give [(Cp*Ru)$_2$(μ_2-η^6:η^6-$C_{20}H_6Me_4$)][X]$_2$ (**6**[X]$_2$) as a dark orange oil or solid (40.0 mg, 85% yield for **6**[PF_6]$_2$). ^{1}H NMR (400.13 MHz, CD_3NO_2, room temperature, **6**[PF_6]$_2$): δ 8.56 (d, ^3J(H,H) = 9.2 Hz, 1H, H9), 8.14 (d, ^3J(H,H) = 9.2 Hz, 1H, H10), 6.82 (d, ^3J(H,H) = 6.0 Hz, 1H, H6), 6.81 (d, ^3J(H,H) = 6.0 Hz, 1H, H1), 6.75 (d, ^3J(H,H) = 6.0 Hz, 1H, H5), 6.73 (d, ^3J(H,H) = 6.0 Hz, 1H, H2), 3.02 (q, ^5J(H,H) = 1.2 Hz, $C_{20}H_6\mathit{Me}_4$, 3H), 2.86 (s, br, $C_{20}H_6\mathit{Me}_4$, 6H), 2.77 (q, ^5J(H,H) = 1.2 Hz, $C_{20}H_6\mathit{Me}_4$, 3H), 1.23 (s, 15H, Cp*), 1.20 (s, 15H Cp*) ppm. ^{13}C{^{1}H} NMR (100.61 MHz, CD_3NO_2, room temperature, **6**[PF_6]$_2$): δ 133.8 (C9), 129.0 (C10), 99.4 (C−Ru), 98.9 (C−Ru), 98.5 (C−Ru), 98.0 (C−Ru), 96.7 (C_5Me_5), 96.5 (C_5Me_5), 96.5 (C−Ru), 96.2 (C−Ru), 95.8 (C−Ru), 93.9 (C−Ru), 85.9 (C1), 85.3 (C2), 85.2 (C5), 84.1 (C6), 17.0 (Me), 16.9 (2 Me), 16.4 (Me), 9.24 ($C_5\mathit{Me}_5$), 9.07 ($C_5\mathit{Me}_5$), 142.7, 137.7, 137.4, 135.4, 134.9, 133.78 (unassigned) ppm. MS: *m/z* 390 ([(Cp*Ru)$_2$(μ_2-η^6:η^6-$C_{20}H_6Me_4$)]$^{2+}$), electrospray in CD_3NO_2. Due to the moisture sensitivity of **6**[X]$_2$, we were unable to obtain satisfactory elemental analyses.

Competition Experiments. A 5 mL flask was charged with corannulene (5.0 mg, 0.020 mmol), 1,2,5,6-tetramethylcorannulene (6.1 mg, 0.020 mmol), $AgPF_6$ (5.3 mg, 0.021 mmol), and only enough [Cp*Ru(μ_3-Cl)]$_4$ (5.4 mg, 0.0050 mmol) to provide 0.020 mmol of {Cp*Ru}$^+$. To the flask was added 1.0 mL of CD_3NO_2, and the solution was stirred for 2 h. The reaction mixture was filtered into an NMR tube and flame-sealed under argon. Relative concentrations of [Cp*Ru(η^6-$C_{20}H_{10}$)]$^+$ ($\mathbf{3}^+$) and [Cp*Ru(η^6-$C_{20}H_6Me_4$)]$^+$ ($\mathbf{5A}^+$ and $\mathbf{5B}^+$) were determined by integration of ^{1}H NMR signals of the C−H protons in **1** and **2** that are coordinated to the {Cp*Ru}$^+$ fragments. Two independent experiments were performed and monitored periodically during three weeks at 25 °C.

Variable-Temperature NMR Studies. Low-temperature solution NMR studies were performed in CD_2Cl_2 solvent on a Bruker AC-200 spectrometer equipped with a Bruker BVT-1000 variable-temperature unit. High-temperature solution NMR studies were undertaken in CD_3NO_2 solvent on a DRX-400 spectrometer, also equipped with a Bruker BVT-1000 variable-temperature unit.

X-ray Structure Determinations of 3[SbF_6]·Et_2O and 4[SbF_6]$_2$·2CH_2Cl_2. Orange crystals of the complex **3**[SbF_6]·Et_2O suitable for an X-ray diffraction study were obtained by layering a methylene chloride solution of the complex with diethyl ether in an 8 mm width Schlenk tube and storing at −25 °C overnight. Orange crystals of complex **4**[SbF_6]$_2$·2CH_2Cl_2 suitable for an X-ray diffraction study were grown by recrystallization from a saturated CH_2Cl_2 solution of the complex that was surrounded by hexanes and stored at −25 °C for 2 weeks.

The crystals of both complexes decomposed within seconds if they were removed from the crystallization solvents. Therefore, they were surrounded by premixed epoxy glue under a layer of the mother liquor and immediately mounted on a goniometer head under a stream of cold nitrogen and centered in the X-ray beam using a video camera. Crystal evaluation and data collection were performed at 193 K on a Bruker CCD-1000 diffractometer with Mo Kα (λ = 0.710 73 Å) radiation and a detector-to-crystal distance of 5.03 cm. The data were collected using the full-sphere routine and were corrected for Lorentz and polarization effects. Absorption corrections were based on fitting a function to the empirical transmission surface, as sampled by multiple equivalent measurements[13] using SADABS software.[14] The structure solutions were accomplished by direct methods. All non-hydrogen atoms were refined by using a full-matrix anisotropic approximation. Hydrogen atoms were placed in the structure factor calculation at idealized positions and were allowed to ride on the neighboring atoms with relative isotropic displacement coefficients.

In **3**[SbF_6]·Et_2O, one $\mathbf{3}^+$ cation, one SbF_6^- anion (distributed in three nonequivalent ordered special positions with occupancy factors 1/6, 2/6, and 1/2, giving three crystallographically nonequivalent positions for Sb and seven for F atoms), and one Et_2O solvent molecule were found in an asymmetric unit of the rhombohedral cell. The symmetry and space group determinations for **4**[SbF_6]$_2$·2CH_2Cl_2 led to the very common *C*2/*c* space group. No unusual obstacles were found in the data reduction, the direct methods solution, or the full-matrix refinement. Half of a positively charged $\mathbf{4}^{2+}$ cation (in a special position on a 2-fold axis), an isolated SbF_6^- counteranion in a general position, and one CH_2Cl_2 solvent molecule were found in an asymmetric unit of the *C*-centered monoclinic cell. All geometrical parameters, thermal displacement coefficients,

(13) Blessing, R. H. *Acta Crystallogr., Sect. A* **1995**, *A51*, 33.
(14) All software and sources of the scattering factors are contained in the SHELXTL (version 5.1) program library (G. M. Sheldrick, Bruker Analytical X-ray Systems, Madison, WI).

and refinement results were found to be reasonable; however, a full structure solution was also performed for a primitive cell with the lowest triclinic space group ($P1$) to avoid geometrical uncertainties, due to possible errors in the symmetry and space group determinations. This solution led to the same essentially flat conformation for the corannulene moiety.

Computational Details. The calculations were performed by employing Spartan 4.0[15] and Gaussian03[16] program packages. Hybrid density functional theory (HDFT) methods were used at the B3LYP level: i.e., Becke's three-parameter hybrid exchange functional[17] in combination with the Lee−Yang−Parr nonlocal correlation functional.[18] Geometry optimization was performed by employing a standard 6-31G(D) basis set for all carbon and hydrogen atoms, while the Hay and Wadt pseudopotential basis set[19] was used for ruthenium atoms (Becke3LYP/GEN). The calculations were performed for $[Cp^*Ru(\eta^6\text{-}C_{20}H_{10})]^+$ ($\mathbf{3}^+$) and $[(Cp^*Ru)_2(\eta^6\text{-}C_{20}H_{10})]^{2+}$ ($\mathbf{4}^{2+}$). To assess the influence of the counteranions on the relative stabilities of the complexes, limited studies of exo and endo $\mathbf{3}^+(PF_6^-)$, exo−endo $\mathbf{4A}^{2+}(PF_6^-)_2$, and exo−exo $\mathbf{4B}^{2+}(PF_6^-)_2$ were undertaken (see infra). The counteranions (PF_6^-) were added at randomly chosen locations to the HDFT-optimized geometries of $\mathbf{3}^+$ or $\mathbf{4}^{2+}$, and the geometry optimization was performed for these complexes with a frozen geometry of the cationic cores using the semiempirical PM3 method,[20] which produced several distinct ionic pairs (or ionic triplets). Those of lowest energies were selected, and the full geometry optimization was then performed for them at the Becke3LYP/GEN level.

Results and Discussion

Synthesis and Structural Characterization of $[Cp^*Ru(\eta^6\text{-}C_{20}H_{10})]^+$ ($\mathbf{3}^+$). The first characterization (by NMR spectroscopy) of an η^6-coordinated corannulene complex, $[Cp^*Ru(\eta^6\text{-}C_{20}H_{10})][O_3SCF_3]$, was reported by Siegel, O'Connor, and co-workers.[7] Their synthetic procedure involved combining $[Cp^*Ru(NCMe)_3][O_3SCF_3]$, the source of the $\{Cp^*Ru\}^+$ fragment, with corannulene in CD_2Cl_2 solvent. In order for the reaction to proceed to completion, it was necessary to remove the CD_2Cl_2 solvent and the displaced MeCN ligands under vacuum. Apparently, the presence of acetonitrile in solution prevented complete conversion to $[Cp^*Ru(\eta^6\text{-}C_{20}H_{10})]^+$. The η^6 complexes $[Cp^*Ir(\eta^6\text{-}C_{20}H_{10})][BF_4]_2$ and $[Cp^*Ir(\eta^6\text{-}C_{20}H_6Me_4)][BF_4]_2$ were prepared similarly by combining $[Cp^*Ir(acetone)_3][BF_4]_2$ with **1** or **2** in nitromethane solvent.[8] On the other hand, the corannulene complexes did not form when $[Cp^*Ir(acetone)_3]^{2+}$ was reacted with **1** or **2** in acetone solvent. From these results, it is apparent that acetonitrile and acetone, although weakly coordinating, compete with corannulene for coordination to the metal fragments.

Our solution to the problem of competing ligands was to use a more reactive source of the $\{Cp^*Ru\}^+$ fragment, one without acetonitrile ligands, and to use a more weakly coordinating solvent. The complex $[Cp^*Ru(\mu_3\text{-}Cl)]_4$ was used as the $\{Cp^*Ru\}^+$ source[12] and CD_3NO_2 as the solvent. When $[Cp^*Ru(\mu_3\text{-}Cl)]_4$ reacts with 4 equiv of Ag^+ and corannulene in CD_3NO_2 solvent under an argon atmosphere at room temperature, $[Cp^*Ru(\eta^6\text{-}C_{20}H_{10})]^+$ ($\mathbf{3}^+$) is formed in nearly quantitative yield within 15 min. Although the $[Cp^*Ru(\eta^6\text{-}C_{20}H_{10})][X]$ complexes ($X = BF_4^-$, PF_6^-, SbF_6^-) were isolated, they are very sensitive to moisture. The previously reported $[Cp^*Ru(\eta^6\text{-}C_{20}H_{10})][O_3SCF_3]$ was assigned a structure in which the $\{Cp^*Ru\}^+$ unit is η^6-coordinated to corannulene on the basis of solution ^1H and ^{13}C NMR studies.[7] The same report suggested on the basis of a theoretical investigation that the $\{Cp^*Ru\}^+$ group was bound on the exo side of the corannulene, although there were no experimental data to support that conclusion.

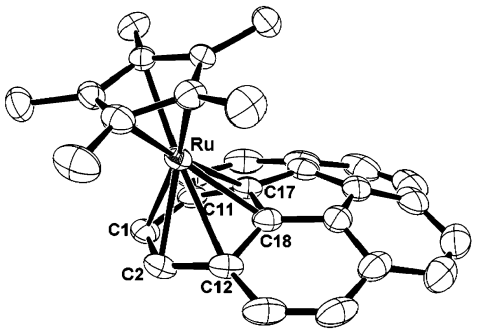

Figure 2. Thermal ellipsoid drawing of the $\mathbf{3}^+$ cation in $[Cp^*Ru(\eta^6\text{-}C_{20}H_{10})][SbF_6]$ ($\mathbf{3}[SbF_6]$). Ellipsoids are shown at the 30% probability level; hydrogen atoms are omitted for clarity. Selected bond distances (Å): Ru1−C1, 2.221(7); Ru1−C2, 2.211(7); Ru1−C12, 2.361(8); Ru1−C18, 2.222(8); Ru1−C17, 2.231(8); Ru1−C11, 2.382(7).

After numerous attempts, X-ray-quality crystals of $\mathbf{3}[SbF_6]\cdot Et_2O$ were obtained. The molecular structure (Figure 2) of the cation in $\mathbf{3}[SbF_6]\cdot Et_2O$ shows that the $\{Cp^*Ru\}^+$ unit is η^6 coordinated to the exo side of corannulene, as the earlier theoretical studies predicted. Of special interest is the partial flattening of the corannulene. This distortion of the corannulene curvature is most evident in the π-orbital axis vector (POAV) analysis,[21] which is a method of quantifying the curvature of carbon networks in nonplanar ring systems. In free corannulene, the five core carbon atoms are the most pyramidalized, having POAV values of 8.4°, while the five rim quaternary carbon atoms are less pyramidalized and have POAV values of 3.8° (Figure 3). In $\mathbf{3}^+$, the two core carbons bonded to Ru have POAV angles that are slightly reduced to 6.6 and 6.8°, as compared with the other three core carbons that have POAV values (8.4, 7.8, 8.3°) that are similar to those of free corannulene. The two rim quaternary carbon atoms that are coordinated to $\{Cp^*Ru\}^+$ also have smaller POAV values (2.0, 1.5°) than in free **1** (3.8°), while those that are not attached to the $\{Cp^*Ru\}^+$ unit have POAV values (4.1, 4.4, 3.4°) that are similar to those in free **1**.

In the previously reported structure of $[(Cp^*Ru)_2(\mu_2\text{-}\eta^6\text{:}\eta^6\text{-}C_{20}H_{10})][PF_6]_2$ ($\mathbf{4}[PF_6]_2$),[9] it was found that coordination of η^6-$\{Cp^*Ru\}^+$ fragments to both the exo and endo sides of the bowl reduced substantially the curvature of the corannulene ligand. The POAV values (Figure 3) for the core carbons (3.5, 3.7°) and the rim quaternary carbon atoms (0.8, 0.5°) bonded to the exo $\{Cp^*Ru\}^+$ unit were smaller than these values for the

(15) *Spartan'04*; Wavefunction, Inc.; Irvine, CA.
(16) Frisch, M. J.; et al. *Gaussian 03,* Revision B.03; Gaussian, Inc.: Pittsburgh, PA, 2003.
(17) Becke, A. D. *J. Chem. Phys*. **1993**, *98*, 5648.
(18) Lee, C.; Yang, W.; Parr, R. G. *Phys. Rev*. **1988**, *B37*, 785.
(19) Hay, P. J.; Wadt, W. R. *J. Phys. Chem*. **1985**, *82*, 299.
(20) (a) Stewart, J. J. P. *J. Comput. Chem.* **1989**, *10*, 209. (b) The PM3 method embedded in the Spartan04[15] package was used.
(21) (a) Haddon, R. C.; Scott, L. T. *Pure Appl. Chem.* **1986**, *58*, 137. (b) Haddon, R. C. *J. Phys. Chem.* **1987**, *91*, 3719. (c) Haddon, R. C. *Acc. Chem. Res.* **1988**, *21*, 243. (d) Haddon, R. C. *J. Am. Chem. Soc.* **1990**, *112*, 3385. (e) Haddon, R. C. *Science* **1993**, *261*, 1545.

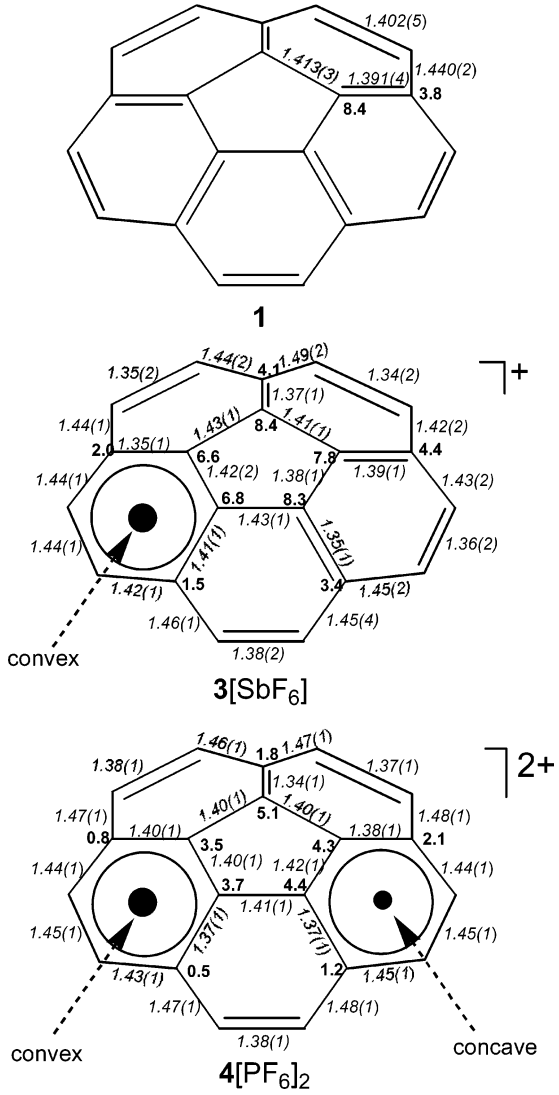

Figure 3. POAV pyramidalization angles (in boldface; deg) and C−C bond lengths (Å) in corannulene (**1**),[4] [Cp*Ru(η^6-$C_{20}H_{10}$)][SbF_6]·Et_2O (**3**[SbF_6]), and [(Cp*Ru)$_2$(μ_2-η^6:η^6-$C_{20}H_{10}$)][PF_6]$_2$·$4CH_2Cl_2$ (**4**[PF_6]$_2$).[9] Only the carbon atoms of corannulene are shown.

core (4.4 and 4.3°) and the rim quaternary carbons (2.1 and 1.2°) bonded to the endo {Cp*Ru}$^+$ units. Moreover, POAV values for the core (5.1°) and rim quaternary carbon atoms (1.8°) that are not coordinated to a {Cp*Ru}$^+$ group were smaller in **4**[PF_6]$_2$ than in free corannulene. The significant changes in the POAV angles of corannulene upon η^6 coordination to {Cp*Ru}$^+$ in both **3**[SbF_6] and **4**[PF_6]$_2$ are in contrast with the structures of the η^2 corannulene complexes [[$Rh_2(O_2CCF_3)_4]_m$·$(C_{20}H_{10})_n$] (m:n = 1:1, 3:2) and [Ag($C_{20}H_{10}$)]$^+$ and [$Ag_2(C_{20}H_{10})]^{2+}$, where no significant changes in the structure of the corannulene were observed.[10,11]

A parameter that is used to describe the overall curvature of a buckybowl is the bowl depth, which is the distance between the centroid of the five core carbon atoms and the plane defined by the 10 tertiary rim carbon atoms. In free corannulene, the bowl depth is 0.87 Å,[3b,4] while it is 0.78 Å in **3**[SbF_6]. The even greater flattening of the corannulene in **4**[PF_6]$_2$ is evident in its bowl depth of only 0.42 Å.

The flattening of corannulene must be accompanied by other structural changes that relieve the strain in the bowl. There are several changes in C−C bond distances (Figure 3) in **3**[SbF_6] as compared with those in **1** that illustrate the effect of {Cp*Ru}$^+$ coordination on the bowl shape. Although the C17−C18 distance (Figure 2) in the five-carbon core is essentially the same in **3**[SbF_6] (1.42(2) Å) as it is in **1** (1.413(3) Å), the C1−C2 distance on the rim of **3**[SbF_6] is 1.44(1) Å, as compared with 1.402(5) Å in **1**. This lengthening of C1−C2 caused by {Cp*Ru}$^+$ coordination relieves strain in the curved bowl, which allows it to become more planar. A similar lengthening (1.45(1) Å) of C−C distances for the carbon atoms bonded to the exo and endo {Cp*Ru}$^+$ units was also observed in **4**[PF_6]$_2$ (Figure 3).[9] Such C−C bond length increases have been reported for many other η^6-arene metal complexes and are explained by charge transfer between the arene and metal complex that results in a net reduction in C−C bond orders.[22]

In contrast to the lengthening of Ru-coordinated rim C−C bond distances, the noncoordinated rim C−C units in **3**[SbF_6] have C−C distances (1.35(2), 1.34(2), 1.36(2), 1.38(2) Å) shorter than that in free corannulene (1.402(5) Å). This trend is also observed in the previously reported structure of **4**[PF_6]$_2$, where the uncoordinated rim C−C bond lengths are 1.38(1), 1.37(1), and 1.38(1) Å. This decrease in C−C bond lengths can be rationalized by assuming that six π electrons are localized in the six-membered rings coordinated to {Cp*Ru}$^+$. The remaining π electrons in the corannulene ligand may then be localized in alternate single and double C−C bonds, as shown in Figure 3. Such localization of electron density in noncoordinated portions of polyaromatic hydrocarbons that are η^6-coordinated to a transition-metal fragment have been observed in several other complexes.[22]

Another interesting feature of the carbon framework in **3**[SbF_6] is the folding of the six-membered ring to which the {Cp*Ru}$^+$ unit is coordinated. The fold occurs along the C11−C12 vector (Figure 2) in a way that moves C1 and C2 up toward the Ru, resulting in a 12° angle between the planes defined by C1, C2, C12, C11 and C12, C18, C17, C11. All of the noncoordinated six-membered rings in **3**[SbF_6] are folded similarly, with fold angles in the range 8.2−12.6°. Moreover, the six-membered rings in free corannulene are folded in a similar manner, with fold angles of 8.8−11.2°.[4] However, in **4**[PF_6]$_2$, the fold angle of the six-membered ring coordinated to the exo {Cp*Ru}$^+$ unit is only 7.8°, while that for the ring coordinated to the endo {Cp*Ru}$^+$ is 5.6°. The fold angles (6.4−8.1°) of the noncoordinated six-membered rings in **4**[PF_6]$_2$ are also smaller than those in either **1** or **3**[SbF_6].

In **3**[SbF_6] (Figure 2), the Ru−C distances are shortest to C1 (2.221(7) Å), C2 (2.211(7) Å), C17 (2.231(8) Å), and C18 (2.222(8) Å) and significantly longer to C11 (2.382(7) Å) and C12 (2.361(8) Å), which reflects folding of the ring along the C11−C12 vector as described above. This same pattern of Ru−C distances is observed in **4**[PF_6]$_2$ for the {Cp*Ru}$^+$ unit bonded to the exo face,[9] where the Ru−C distances are also shortest to C1 (2.219(7)), C2 (2.214(6)), C17 (2.209(6)), and C18 (2.209(6)) and the

(22) Hubig, S. M.; Lindeman, S. V.; Kochi, J. K. *Coord. Chem. Rev.* **2000**, *200−202*, 831.

C11 (2.343(7)) and C12 (2.346(6)) distances are longer. On the other hand, the Ru−C bond distance pattern for the endo $\{Cp^*Ru\}^+$ unit in **4**$[PF_6]_2$ exhibits short Ru−C distances (2.176(7) and 2.169(7) Å) to the two rim carbons (C5 and C6 in Figure 1) but longer Ru−C bonds (2.263(7), 2.266(7), 2.264(7), and 2.276(7) Å) to the other four carbon atoms C13, C14, C19, and C20. The different Ru−C bond lengths to the coordinated arene rings of **3**$[SbF_6]$ and **4**$[PF_6]_2$ are in contrast to those reported for other $[Cp^*Ru(\eta^6\text{-arene})]^+$ complexes such as $[Cp^*Ru(\eta^6\text{-}C_6(CH_3)_6)]^+$, in which all of the Ru−C bond distances are very similar (2.18−2.22 Å).[12]

All of the structural changes of the corannulene unit induced by complexation with $\{Cp^*Ru\}^+$ as found in the crystal of **3**$[SbF_6]\cdot Et_2O$ are closely reproduced by our Becke3LYP/GEN calculations performed for $\mathbf{3}^+$. Thus, the observed elongation of the rim CH−CH bond of the metal-coordinated ring is reflected in the calculated structure (1.44 Å as compared to 1.39 Å for the remaining four CH−CH bonds in $\mathbf{3}^+$ and in corannulene at the same level of theory). Generally, the calculated C−C bond distances in $\mathbf{3}^+$ are ca. 0.01 Å longer than the X-ray-determined values. Also, the calculations predict that the Ru−C11 and Ru−C12 bond lengths are the longest (2.49 Å), while the remaining four bonding Ru−C distances are significantly shorter (2.29 Å for Ru−C1 and Ru−C2 and 2.35 Å for Ru−C17 and Ru−C18). A recent computational study[23] of the unknown $(OC)_3Cr(\eta^6\text{-}C_{20}H_{10})$ gives the same pattern of Cr−C distances and an elongated rim CH−CH bond in the coordinated ring. In accord with crystal data, the calculated structure of $\mathbf{3}^+$ exhibits a slight flattening of the corannulene bowl as compared to **1**. Thus, POAV pyramidalization angles for the five core atoms (C16−C20) range from 7.7 to 8.5° (average 8.1°), only slightly higher than the crystal structure values (6.6−8.4°, average 7.7°). The calculated pyramidalization angle for the coordinated carbons C11 and C12 (1.9°) also compare favorably to the crystal structure values (1.5 and 2.0°, respectively).

The exo coordination of the $\{Cp^*Ru\}^+$ group observed in the crystal of **3**$[SbF_6]\cdot Et_2O$ is also predicted by the computational model for $\mathbf{3}^+$. The exo haptomer of the $[CpRu(\eta^6\text{-}C_{20}H_{10})]^+$ cation was previously calculated by Baldridge et al. to be ca. 6 kcal/mol more stable than the endo isomer.[7] It was also suggested that the presence of five methyl groups in Cp* would further increase the preference for the exo haptomer of $[Cp^*Ru(\eta^6\text{-}C_{20}H_{10})]^+$ ($\mathbf{3}^+$), due to repulsions between the methyl groups and the rim hydrogen atoms of the corannulene in the endo haptomer. We found the exo $\mathbf{3}^+$ to be more stable than the endo isomer by 7.6 kcal/mol, while the exo preference for the simpler $[CpRu(\eta^6\text{-}C_{20}H_{10})]^+$, where $Cp = \eta^5\text{-}C_5H_5$, is calculated to be 6.7 kcal/mol at the same level of theory. The slight difference in the calculated exo preferences (7.6 and 6.7 kcal/mol) shows that steric congestion in the endo complex $\mathbf{3}^+$ is of only minor importance. This conclusion is also supported by an examination of the calculated nonbonding distances between the methyl group atoms of the Cp* ligand and the rim atoms of corannulene in $\mathbf{3}^+$, which are all larger than the sum of the respective van der Waals radii, the shortest C···C distance being 3.76 Å. Introduction of the PF_6^- counteranion into the computational model does not change the exo vs endo preference. The lowest energy *exo*-**3**$[PF_6]$ isomer is calculated to be more stable than the "best" endo counterpart by 7.8 kcal/mol: i.e., very close to 7.6 kcal/mol found for $\mathbf{3}^+$ in the absence of an anion.

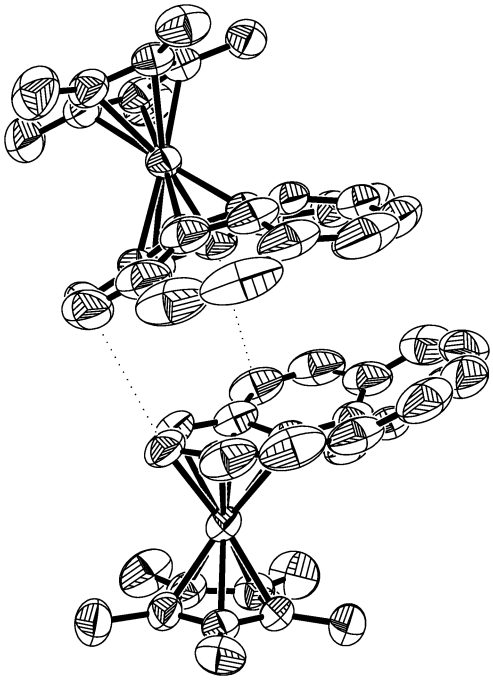

Figure 4. ORTEP diagram of the packing arrangement between two $\mathbf{3}^+$ units in **3**$[SbF_6]\cdot Et_2O$. Ellipsoids are drawn at the 30% probability level; hydrogen atoms, anions, and solvent molecules are not shown for clarity. The intermolecular distances of ~3.4 Å are shown by dashed lines. The angle between the cen-C_5−cen-C_5 vector and the C_5 core plane is 76.1°.

The extended structure (Figure 4) of $[Cp^*Ru(\eta^6\text{-}C_{20}H_{10})][SbF_6]$ (**3**$[SbF_6]$) shows that two $[Cp^*Ru(\eta^6\text{-}C_{20}H_{10})]^+$ cations arrange themselves in such a way that the concave faces of the corannulene ligands face each other, which leaves a vacant pocket between them. Although diethyl ether molecules are present elsewhere in the crystal lattice, none was observed inside the cavity. The shortest carbon-to-carbon distance between carbon atoms on the two $[Cp^*Ru(\eta^6\text{-}C_{20}H_{10})]^+$ units is ~3.4 Å, which is sufficiently long to indicate that there is no bonding between the corannulene groups.

Synthesis and Characterization of $[Cp^*Ru(\eta^6\text{-}C_{20}H_6Me_4)]^+$ ($\mathbf{5}^+$). When $[Cp^*Ru(\mu_3\text{-Cl})]_4$ reacts with 4 equiv of 1,2,5,6-tetramethylcorannulene (**2**) and 4 equiv of a AgX salt (X = BF_4^-, PF_6^-, SbF_6^-) at room temperature in CD_3NO_2 solvent, $[Cp^*Ru(\eta^6\text{-}C_{20}H_6Me_4)]^+$ ($\mathbf{5}^+$) forms within 15 min. Two isomers of the product were observed by solution ^1H NMR spectroscopy in a 2:1 ratio for $\mathbf{5A}^+$:$\mathbf{5B}^+$ (Figure 1). Recrystallization of the mixture of $\mathbf{5A}^+$ and $\mathbf{5B}^+$ often resulted in the enrichment of one isomer over the other, which aided in the spectroscopic assignments; however, attempts to obtain X-ray-quality crystals were unsuccessful. The ^1H NMR signals of a sample enriched in $\mathbf{5B}^+$ are all ~0.1 ppm downfield of those in the initial 2:1 mixture; the cause of this shift is not clear. $^1H-^1H$ COSY, $^1H-^{13}C$ HETCOR, and $^1H-^1H$ NOESY experiments, along with relative shifts in

(23) Stoddart, M. W.; Brownie, J. H.; Baird, M. C.; Schmider, H. L. *J. Organomet. Chem.* **2005**, *690*, 3440.

^{1}H NMR signals, were used to make tentative proton and carbon assignments in spectra of the mixtures of the **5A**$^+$ and **5B**$^+$ isomers (Figure 1). The hydrogen signals for H5, H6, H9, and H10 of the major isomer (**5A**$^+$) occur as doublets at 8.23, 8.07, 7.94, and 7.62 ppm. Upfield signals between 6.46 and 6.42 ppm that arise from second-order AB coupling are assigned to H1 and H2. The four methyl groups in the $C_{20}H_6Me_4$ unit of **5A**$^+$ are observed as four signals between 2.9 and 2.6 ppm. The middle two methyl signals are singlets and are located in the same region (although better resolved) as those for the methyl signals of free **2** (2.75, 2.74 ppm). The other two methyl group signals are unresolved quartets (J(H,H) = 0.8 Hz); one is shifted ~0.1 ppm upfield and the other ~0.1 ppm downfield from those of free **2**. The more symmetrical minor isomer, **5B**$^+$, has a much simpler ^{1}H NMR spectrum. Doublets at 8.05 and 7.98 ppm may be assigned to H6, H7 and H5, H8, while a singlet at 6.45 ppm may be assigned to H1 and H2. There are two methyl signals; one is shifted ~0.1−0.2 ppm upfield, while the other is shifted ~0.1 ppm downfield of those in free **2**. These methyl group signals both appear as unresolved quartets with J(H,H) = 0.8 Hz. In both **5A**$^+$ and **5B**$^+$, only one peak is observed for the Cp* methyl groups. The significant upfield shifts (1.3−1.5 ppm) of the signals assigned to the coordinated C−H groups in **5A**$^+$ and **5B**$^+$ are similar in magnitude to those observed in ^{1}H NMR spectra of both [Cp*Ru(η^6-$C_{20}H_{10}$)][O_3SCF_3][7] and [(Cp*Ru)$_2$(μ_2-η^6:η^6-$C_{20}H_{10}$)][PF_6]$_2$ (**4**[PF_6]$_2$)[9] and are typical of other [Cp*Ru(η^6-arene)]$^+$ compounds.[12,24] It is interesting that methyl signals of **5A**$^+$ and **5B**$^+$ appear as quartets, with small coupling constants (0.8 Hz), presumably the result of ^5J(H,H) homoallylic coupling[25] between methyl groups. The pattern of singlets and unresolved quartets for the methyl groups of **2** in **5A**$^+$ suggests that this coupling is only observed for those methyl groups that are located on rings adjacent to those containing a coordinated η^6-{Cp*Ru}$^+$ group.

There was no NMR evidence for the formation of other isomers in the reactions of **2** with [Cp*Ru(μ_3-Cl)]$_4$ and AgX. Even after the initial CD_3NO_2 solution of the isomers was heated to 101 °C for 24 h, the ratio of **5A**$^+$ to **5B**$^+$ remained 2:1. In attempts to determine whether **5A**$^+$ and **5B**$^+$ could be interconverted, a CD_3NO_2 solution containing them was allowed to stand for 2 weeks at room temperature, and no change was observed in the **5A**$^+$:**5B**$^+$ ratio. The **5A**$^+$:**5B**$^+$ isomer ratio also remained unchanged (2:1) when the mixture of isomers in CD_3NO_2 was heated at 50 °C for 2 days followed by recording the ^{1}H NMR spectrum at 50 °C. Only by recrystallization of the mixture of isomers **5A**[SbF_6] and **5B**[SbF_6] was the ratio changed from 2:1. The **5A**$^+$:**5B**$^+$ ratio in the solids resulting from these recrystallizations ranged from 9:1 to 3:7. All of these studies show that **5A**$^+$ and **5B**$^+$ do not interconvert under the above conditions. The 2:1 ratio of **5A**$^+$:**5B**$^+$ formed initially may simply be a result of the types of nonmethylated rings in **2**; there are two of the adjacent rings but only one of the type between methylated rings.

This inability of the {Cp*Ru}$^+$ group to migrate from one six-membered ring of **2** to another may account for the fact that an isomer (**5C**$^+$) in which the {Cp*Ru}$^+$ unit is on a methylated ring is not observed. Ring migration of the η^6-{Cp*Ru}$^+$ group is reported in the reaction of [Cp*Ru(NCMe)$_3$][O_3SCF_3] with acecorannulene,[26] a corannulene derivative that has three differently curved six-membered rings, in CD_2Cl_2. The migration of the {Cp*Ru}$^+$ group across acecorannulene in that study may be catalyzed by residual acetonitrile that remains in the reaction mixture. In the reaction of [Cp*Ir(acetone)$_3$]$^{2+}$ with **2**,[8] the major isomer of [Cp*Ir(η^6-$C_{20}H_6Me_4$)]$^{2+}$ that forms initially is that in which the {Cp*Ir}$^{2+}$ unit binds to one of the equivalent, adjacent nonmethylated rings. However, within 6 h, this isomer completely rearranges to the isomer in which {Cp*Ir}$^{2+}$ is coordinated to a methylated ring. The total absence of such an isomer of **5**$^+$ is possibly due to the fact that migration of the {Cp*Ru}$^+$ unit in this system, in which there is no residual acetonitrile or acetone to facilitate isomerization, is very slow. It is rather unlikely that **5C**$^+$ is thermodynamically unstable with respect to **5A**$^+$ and **5B**$^+$, since according to our calculations the stabilities of all three isomers of *exo*-**5**$^+$ are very similar. At the B3LYP/gen level of theory, **5A**$^+$ is found to be the most stable isomer, with **5B**$^+$ and **5C**$^+$ higher in energy by only 0.04 and 0.11 kcal/mol, respectively.

In an attempt to determine whether **1** or **2** binds more strongly to {Cp*Ru}$^+$, a competition experiment in which 1 equiv of **1**, 1 equiv of **2**, and 1 equiv of {CpRu}$^+$ were reacted. The reaction was initiated by adding CD_3NO_2 solvent to a mixture of the solids **1**, **2**, [Cp*Ru(μ_3-Cl)]$_4$, and $AgPF_6$, in a 1:1:0.25:1 molar ratio. The reaction mixture was stirred at room temperature for 2 h before being filtered into an NMR tube and sealed. The tube at room temperature was monitored periodically over a period of 3 weeks. The relative concentrations of the monometalated products **3**$^+$, **5A**$^+$, and **5B**$^+$ were determined by integration of the signals in the ^{1}H NMR spectra between 6.5 and 6.3 ppm, corresponding to the hydrogens on those rings to which the {Cp*Ru}$^+$ fragments are bound. No products with two {Cp*Ru}$^+$ units coordinated to **1** or **2** were observed. Results of two independent runs showed that the ratio **3**$^+$:(**5A**$^+$ + **5B**$^+$) was 1:2.8 and 1:3.0 for the two runs and that this ratio remained unchanged after the first measurement immediately following the reaction. Because there was no change in this ratio with time and because studies of the isomerization of **5A**$^+$ and **5B**$^+$ showed that the {Cp*Ru}$^+$ groups are not labile, it seems likely that the observed 1:2.9 ratio of **3**$^+$ to **5**$^+$ indicates that {Cp*Ru}$^+$ reacts kinetically (including the rates of dissolution of **1** and **2**) more rapidly with **2** than with **1** under the conditions of this study. However, the ratio does not establish the relative thermodynamic stabilities of **3**$^+$ and **5**$^+$.

Synthesis and Characterization of [(Cp*Ru)$_2$(μ_2-η^6:η^6-$C_{20}H_{10}$)][SbF_6]$_2$ (4[SbF_6]$_2$) and [(Cp*Ru)$_2$(μ_2-η^6:η^6-$C_{20}H_6Me_4$)]$^{2+}$ (6^{2+}). The compound [(Cp*Ru)$_2$(μ_2-η^6:η^6-$C_{20}H_{10}$)][SbF_6]$_2$ (**4**[SbF_6]$_2$) was synthesized in a manner identical with that previously reported for the BF_4^- and

(24) Xia, A.; Selegue, J. P.; Carrillo, A.; Brock, C. P. *J. Am. Chem. Soc.* **2000**, *122*, 3973.

(25) Nelson, J. H. *Nuclear Magnetic Resonance Spectroscopy*; Pearson Education: Upper Saddle River, NJ, 2003; pp 137−138.

(26) Seiders, T. J.; Baldridge, K. K.; O'Connor, J. M.; Siegel, J. S. *Chem. Commun.* **2004**, 950.

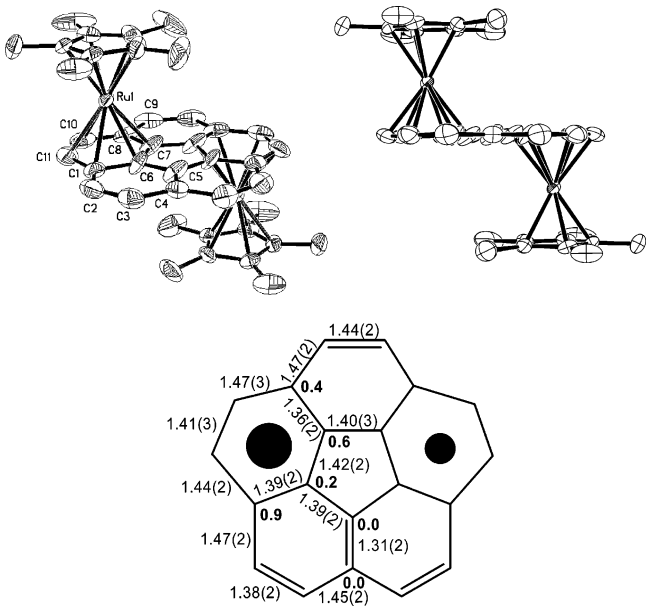

Figure 5. (top) Thermal ellipsoid drawings of the dication in $[(Cp^*Ru)_2(\mu_2\text{-}\eta^6\text{:}\eta^6\text{-}C_{20}H_{10})][SbF_6]_2\cdot 2CH_2Cl_2$ (**4**$[SbF_6]_2$). Ellipsoids are shown at the 30% probability level; hydrogen atoms are omitted for clarity. Selected bond distances (Å): Ru−C10, 2.189(15); Ru−C11, 2.189(15); Ru−C6, 2.228(15); Ru−C7, 2.220(13); Ru−C1, 2.331(15); Ru−C8, 2.304(15). (bottom) POAV pyramidalization angles (in boldface, deg) and C−C bond lengths (Å).

PF_6^- salts **4**$[BF_4]_2$ and **4**$[PF_6]_2$,[9] except that $AgSbF_6$ was used as the AgX reagent. Unlike the previously reported structure of **4**$[PF_6]_2\cdot 4CH_2Cl_2$,[9] the structure (Figure 5) of **4**$[SbF_6]_2\cdot 2CH_2Cl_2$ contains $\{Cp^*Ru\}^+$ fragments that are crystallographically equivalent, as a result of a C_2 axis of symmetry along the C4−C5 bond. The relatively large *R* factor (8.9%) for **4**$[SbF_6]_2\cdot 2CH_2Cl_2$ seems to be related to significant thermal motion in the core five-membered ring of the corannulene unit, as two other independently prepared crystal samples, obtained under the same crystallization conditions, had similarly large *R* factors, but with the same symmetry and solvent-to-complex ratio. The structure reveals a corannulene subunit that no longer has a bowl shape; it is more like a "plate". The C_{20} unit is very nearly flat, as the RMS deviation from the "best" plane is only 0.013 Å. There are, however, small distortions from planarity, as indicated by the POAV values (0.6 and 0.2° in Figure 5) for the core carbon atoms that are attached to $\{Cp^*Ru\}^+$. These numbers are significantly smaller than those in **4**$[PF_6]_2\cdot 4CH_2Cl_2$, which had values of 3.5 and 3.7° for the core carbon atoms attached to the exo $\{Cp^*Ru\}^+$ fragment and 4.3 and 4.4° for the core carbons attached to the endo $\{Cp^*Ru\}^+$ fragment. The POAV values for the rim quaternary carbon atoms attached to the $\{Cp^*Ru\}^+$ unit in **4**$[SbF_6]_2\cdot 2CH_2Cl_2$ (0.4 and 0.9°) are the same as those in the corannulene ring bound to the exo $\{Cp^*Ru\}^+$ fragment in **4**$[PF_6]_2$ (0.5 and 0.8°) but smaller than those for the ring bound to the endo $\{Cp^*Ru\}^+$ fragment (2.1 and 1.2°) (Figure 3). That the corannulene is not completely flat is indicated by the slightly longer Ru−C distances to C1 (2.33(2) Å) and C8 (2.30(2) Å) as compared to the distance to C6 (2.23(2) Å), C7 (2.22(1) Å), C10 (2.19(2) Å), and C11 (2.19(2) Å). Thus, the ring is folded along the C1−C8 vector, as was observed in free corannulene and in the corannulene units in **3**$[SbF_6]$ and **4**$[PF_6]_2$. The fold angle, defined as the dihedral angle between the C1, C6, C7, C8 and C8, C10, C11, C1 planes in Figure 5, for the coordinated six-membered rings decreases in the series of complexes as follows: 12° for **3**$[SbF_6]$, 7.8° for the exo and 5.6° for the endo $\{Cp^*Ru\}^+$ in **4**$[PF_6]_2$, and 1.2° for **4**$[SbF_6]_2$. The observation that the corannulene is much flatter in **4**$[SbF_6]_2\cdot 2CH_2Cl_2$ than in **4**$[PF_6]_2\cdot 4CH_2Cl_2$ shows that the corannulene ligand in $\mathbf{4}^{2+}$ is sufficiently flexible that its shape depends on the lattice energy of the crystals, which is influenced by the anion (PF_6^- vs SbF_6^-) and the number of CH_2Cl_2 molecules (four vs two) in the lattice.

The calculated structure of $\mathbf{4}^{2+}$ exhibits a significantly flattened corannulene bowl, very similar to that found previously in the structure of **4**$[PF_6]_2\cdot 4CH_2Cl_2$.[9] As in $\mathbf{3}^+$, structural features of the corannulene unit observed in the crystal of **4**$[PF_6]_2\cdot 4CH_2Cl_2$ are very well reproduced by the model calculations. In agreement with the X-ray findings, major bond length changes are found in the ruthenium-coordinated rings. This includes elongation of the two CH−CH bonds to 1.451 and 1.448 Å, which are virtually identical with those determined in the crystal structure (1.45 Å) and very similar to that (1.44 Å) found in $\mathbf{3}^+$ (see above). The calculated CH−CH bond lengths of the three noncoordinated rings are in the range 1.393−1.414 Å, again in reasonable agreement with the X-ray data for **4**$[PF_6]_2\cdot 4CH_2Cl_2$ (Figure 3). The POAV pyramidalization angles calculated for the optimized structure of $\mathbf{4}^{2+}$ are in the range 4.1−6.2° (average 5.2°) for the core atoms and 0.2−2.4° (average 1.4°) for the five quaternary rim carbon atoms, while the same angles derived from the crystal structure of **4**$[PF_6]_2\cdot 4CH_2Cl_2$ are 3.5−5.1° (average 4.2°) and 0.5−2.1° (average 1.3°), respectively. The analogous numbers for corannulene (**1**) optimized at the same level of theory are 8.0 and 3.6°, respectively.

The structure of the "flat" corannulene in **4**$[SbF_6]_2\cdot 2CH_2Cl_2$ might be considered as closely related to the transition state for the bowl-to-bowl inversion of $\mathbf{4}^{2+}$. The calculated transition state ($\mathbf{4TS}^{2+}$) also exhibits C_2 symmetry and has a nearly flat corannulene moiety. There is a very close correlation between the calculated bond lengths and angles in $\mathbf{4TS}^{2+}$ and the crystal data for **4**$[SbF_6]_2\cdot 2CH_2Cl_2$. At the B3LYP/GEN level of theory the "flat" $\mathbf{4TS}^{2+}$ is higher in energy than the shallow-bowl minimum energy $\mathbf{4}^{2+}$ by only 1.6 kcal/mol, which makes it reasonable that crystal-packing forces could change the conformation of the corannulene in the **4**$[PF_6]_2\cdot 4CH_2Cl_2$ and **4**$[SbF_6]_2\cdot 2CH_2Cl_2$ crystals.

There are several possible haptomers of $\mathbf{4}^{2+}$, depending upon the location of the two $\{Cp^*Ru\}^+$ units on the corannulene. Due to steric congestion caused by the Cp* units, all endo−endo isomers, as well as the exo−exo isomer with the two $\{Cp^*Ru\}^+$ groups coordinated to adjacent six-membered rings, are eliminated as candidates for low-energy structures. Preliminary semiempirical calculations attempted for these potentially high-energy isomers led either to dissociation of the complex or to corannulene bowl inversion and/or migration of the $\{Cp^*Ru\}^+$ units. At the B3LYP/GEN level of theory, we

investigated four isomers of $\mathbf{4}^{2+}$, i.e., $\mathbf{4A}^{2+}$–$\mathbf{4D}^{2+}$. According to the calculations, the exo–exo haptomer $\mathbf{4B}^{2+}$ is of lowest energy, which is consistent with the exo preference found in $\mathbf{3}^{+}$. The exo–endo isomer $\mathbf{4A}^{2+}$, found in the solid state, is predicted to be higher in energy than $\mathbf{4B}^{2+}$ by 3.3 kcal/mol. The second exo–endo isomer, $\mathbf{4C}^{2+}$, with the two $\{Cp^*Ru\}^+$ units coordinated to adjacent six-membered rings, is significantly less stable than $\mathbf{4B}^{2+}$ by 9.5 kcal/mol. Finally, $\mathbf{4D}^{2+}$, with two metals coordinated to both faces of the same benzene ring, is the least stable of them all and is less stable than $\mathbf{4B}^{2+}$ by 19.5 kcal/mol.

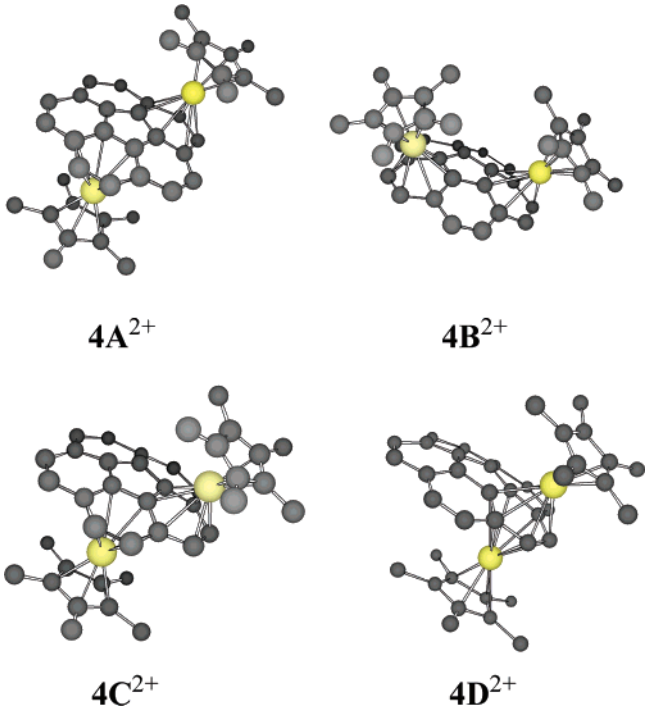

At this point, we can only speculate why the exo–endo structure ($\mathbf{4A}^{2+}$) is represented in the crystals of $\mathbf{4}[PF_6]_2\cdot 4CH_2Cl_2$ and $\mathbf{4}[SbF_6]_2\cdot 2CH_2Cl_2$, while the computational studies indicate that the exo–exo isomer $\mathbf{4B}^{2+}$ is more stable. The introduction of the PF_6^- counteranions into the computational model does not change the relative stabilities significantly, since the "best" ionic triplet of $\mathbf{4B}[PF_6]_2$ is still lower in energy than $\mathbf{4A}[PF_6]_2$ by 1.8 kcal/mol. It is possible that the $\mathbf{4A}^{2+}$ isomer found in the solids is favored by crystal-packing forces. On the other hand, $\mathbf{4A}^{2+}$ may be the isomer that is formed initially in the reaction, and its isomerization to $\mathbf{4B}^{2+}$ is kinetically very slow. The unobservably slow interconversion of isomers $\mathbf{5A}^{+}$ and $\mathbf{5B}^{+}$ is consistent with this possibility.

Like **1**, **2** also reacts with $[Cp^*Ru(\mu_3\text{-}Cl)]_4$ with Ag^+ to give only one isomer of $[(Cp^*Ru)_2(\mu_2\text{-}\eta^6\text{:}\eta^6\text{-}C_{20}H_6Me_4)]^{2+}$ ($\mathbf{6}^{2+}$), in which two $\{Cp^*Ru\}^+$ units are η^6-coordinated to the corannulene framework. Complex $\mathbf{6}^{2+}$ was characterized by its NMR and mass spectra and shown to have the structure in Figure 1. The ^1H NMR spectrum (Figure 6) of the $C_{20}H_6Me_4$ ligand in $\mathbf{6}[PF_6]_2$ shows doublets at 8.56 and 8.14 ppm that are mutually coupled in the COSY NMR spectrum and may be assigned to H9 and H10. There are also four upfield doublets at 6.9–6.7 ppm which are correlated in the COSY spectrum and may be assigned to H1, H2 and H5, H6. A NOESY NMR study of $\mathbf{6}[BF_4]_2$ revealed a correlation between H1 and H10, which is further support for the conclusion that the $\{Cp^*Ru\}^+$ units coordinate to the nonmethylated rings of **2**. There are three methyl signals for $\mathbf{6}[PF_6]_2$ between 3.1 and 2.7 ppm in the ^1H NMR spectrum (Figure 6, bottom). Two of these signals are unresolved quartets that are each integrated to three hydrogens. The third signal is a broad singlet between them corresponding to six hydrogen atoms; all three signals are shifted only slightly downfield (≤0.3 ppm) from that of the methyl groups in free **2**. There are also two separate signals for the methyl groups of the Cp* ligands that are each integrated to 15 hydrogen atoms. The ^1H NMR data indicate that the only isomer formed is that in which both $\{Cp^*Ru\}^+$ units are η^6-coordinated to nonmethylated, nonadjacent six-membered rings (Figure 1). Presumably, the $\{Cp^*Ru\}^+$ units are on opposite sides of the buckybowl ligand, as was observed in the structures of $\mathbf{4}[PF_6]_2\cdot 4CH_2Cl_2$ and $\mathbf{4}[SbF_6]_2\cdot 2CH_2Cl_2$. However, numerous attempts to obtain X-ray-quality crystals of $\mathbf{6}^{2+}$ using various anions and crystallization methods were unsuccessful.

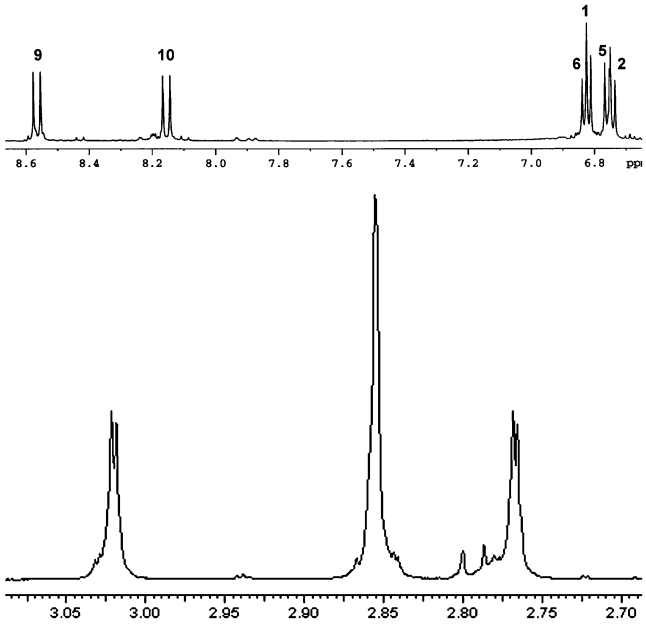

Figure 6. ^1H NMR spectra of the $C_{20}H_6Me_4$ ligand (C–H region, top; $C\text{–}CH_3$ region, bottom) in $[(Cp^*Ru)_2(\mu_2\text{-}\eta^6\text{:}\eta^6\text{-}C_{20}H_6Me_4)][PF_6]_2$ ($\mathbf{6}[PF_6]_2$) in CD_3NO_2.

Corannulene undergoes rapid bowl-to-bowl inversion in solution at room temperature.[27] The inversion barrier ($\Delta G^{\ddagger}$) for corannulene derivatives that are monofunctionalized on the rim by diastereotopic groups, which presumably do not alter the structure of the corannulene unit significantly, is approximately 11 kcal/mol. Experi-

(27) (a) Scott, L. T.; Hashemi, M. M.; Bratcher, M. S. *J. Am. Chem. Soc.* **1992**, *114*, 1920. (b) Sygula, A.; Abdourazak, A. H.; Rabideau, P. W. *J. Am. Chem. Soc.* **1996**, *118*, 339. (c) Seiders, T. J.; Baldridge, K. K.; Grube, G. H.; Siegel, J. S. *J. Am. Chem. Soc.* **2001**, *123*, 517. (d) Seiders, T. J.; Baldridge, K. K.; Elliott, E. L.; Grube, G. H.; Siegel, J. S. *J. Am. Chem. Soc.* **1999**, *121*, 7439. (e) Marcinow, Z.; Sygula, A.; Ellern, A.; Rabideau, P. W. *Org. Lett.* **2001**, *3*, 3527. (f) Grube, G. H.; Elliott, E. L.; Steffens, R. J.; Jones, C. S.; Baldridge, K. K.; Siegel, J. S. *Org. Lett.* **2003**, *5*, 713. (g) Dinadayalane, T. C.; Deepa, S.; Reddy, A. S.; Sastry, G. N. *J. Org. Chem.* **2004**, *69*, 8114. (h) Dinadayalane, T. C.; Deepa, S.; Sastra, G. N. *Tetrahedron Lett.* **2003**, *44*, 4527. (i) Sastry, G. N.; Rao, H. S. P.; Priyakumar, U. D.; Bednarek, P. *Chem. Commun.* **2000**, 843.

mental and theoretical studies indicate that inversion barriers in corannulene derivatives are highly dependent on, and directly proportional to, their curvatures and bowl depths.[26] Those substituents and interactions that lead to a decrease in the curvature and flattening of the buckybowl result in structures with lower barriers to inversion. The previously reported solution NMR spectrum for $[(Cp^*Ru)_2(\mu_2\text{-}\eta^6\text{:}\eta^6\text{-}C_{20}H_{10})][PF_6]_2$ (**4**$[PF_6]_2$) in CD_2Cl_2 contained only one signal for the methyl groups of the Cp* ligands at room temperature. If the inversion were slow on the NMR time scale, one would expect separate signals for the $\{Cp^*Ru\}^+$ units that are on the exo and endo sides of the corannulene. The observation of only one Cp* signal indicates that the inversion is fast or that the corannulene is "flat" in solution, as it is in **4**$[SbF_6]_2 \cdot 2CH_2Cl_2$. Attempts to determine the spectrum of **4**$[PF_6]_2$ at low temperature were not possible, because of its low solubility in CD_2Cl_2. Complex $\mathbf{6}^{2+}$ is much more soluble, and low-temperature NMR studies of it were undertaken in an attempt to determine the inversion barrier of these dimetalated corannulene complexes. The ^1H and ^{13}C NMR spectra of **6**$[PF_6]_2$ in CD_2Cl_2 showed only two signals for the two different $\{Cp^*Ru\}^+$ groups down to 183 K, suggesting that a fast inversion process occurs even at this low temperature or that the corannulene is "flat" in solution. The flattened geometries of the corannulene ligand in the structures of **4**$[PF_6]_2$ and **4**$[SbF_6]_2$ are consistent with either of these interpretations, which are also strongly supported by the very low calculated energy barrier (1.6 kcal/mol) for bowl-to-bowl inversion of the model system $\mathbf{4}^{2+}$.

Conclusions

A new synthetic procedure has been developed for the attachment of one and two η^6-$\{Cp^*Ru\}^+$ fragments to corannulenes in high yields, based on the use of $[Cp^*Ru(\mu_3\text{-}Cl)]_4$ as the source of $\{Cp^*Ru\}^+$ and CD_3NO_2 as the solvent. X-ray structural investigations show that the $\{Cp^*Ru\}^+$ fragment is attached (η^6) to the exo side of corannulene in $[Cp^*Ru(\eta^6\text{-}C_{20}H_{10})][SbF_6]$ (**3**$[SbF_6]$) and that the $\{Cp^*Ru\}^+$ units in $[(Cp^*Ru)_2(\mu_2\text{-}\eta^6\text{:}\eta^6\text{-}C_{20}H_{10})][PF_6]_2$[9] (**4**$[PF_6]_2$) and $[(Cp^*Ru)_2(\mu_2\text{-}\eta^6\text{:}\eta^6\text{-}C_{20}H_{10})][SbF_6]_2$ (**4**$[SbF_6]_2$) are η^6-coordinated to nonadjacent arene rings on opposites sides of corannulene. Coordination of the $\{Cp^*Ru\}^+$ fragments results in significant flattening of the corannulene bowl, which is the likely reason for the low barrier to corannulene inversion in $[(Cp^*Ru)_2(\mu_2\text{-}\eta^6\text{:}\eta^6\text{-}C_{20}H_6Me_4)][PF_6]_2$ (**6**$[PF_6]_2$). The dramatic flattening effect of η^6-$\{Cp^*Ru\}^+$ coordination on the curvature of corannulene may account for the instability of η^6 complexes of fullerene C_{60}. Flattening of part of the rigid C_{60} carbon cage would cause severe strains in other regions of the buckyball.

Acknowledgment. This work was supported by the U.S. Department of Energy Office of Science, Office of Basic Energy Sciences, Chemical Sciences Division, under Contract W-7405-Eng-82 with Iowa State University and through Grant DE-FG02-04ER15514 to Mississippi State University. A.S. thanks the Mississippi Center for Supercomputing for an allotment of computer time.

Supporting Information Available: Text, figures, and tables giving the complete ref 16, ^1H and ^{13}C NMR spectra of **1**, **2**, $\mathbf{5A}^+$, $\mathbf{5B}^+$, and $\mathbf{6}^{2+}$, and calculational results, optimized geometries, and total energies and crystallographic data files (CIF) giving data for the structures of **3**$[SbF_6]$ and **4**$[SbF_6]_2$. This material is available free of charge via the Internet at http://pubs.acs.org.

OM0505458